Localizing quantum phase slips in one-dimensional Josephson junction chains

2013 New J. Phys. 15 095014

(http://iopscience.iop.org/1367-2630/15/9/095014)

New Journal of Physics
The open access journal for physics

Localizing quantum phase slips in one-dimensional Josephson junction chains

Adem Ergül[1,4], Jack Lidmar[2], Jan Johansson[3], Yağız Azizoğlu[1], David Schaeffer[1] and David B Haviland[1]

[1] Nanostructure Physics, Royal Institute of Technology, SE-106 91 Stockholm, Sweden
[2] Theoretical Physics, Royal Institute of Technology, SE-106 91 Stockholm, Sweden
[3] Department of Natural Sciences, University of Agder, Kristiansand, Norway
E-mail: adem@kth.se

New Journal of Physics **15** (2013) 095014 (13pp)
Received 30 May 2013
Published 25 September 2013
Online at http://www.njp.org/
doi:10.1088/1367-2630/15/9/095014

Abstract. We studied quantum phase-slip (QPS) phenomena in long one-dimensional Josephson junction series arrays with tunable Josephson coupling. These chains were fabricated with as many as 2888 junctions, where one sample had a separately tunable link in the middle of the chain. Measurements were made of the zero-bias resistance, R_0, as well as current–voltage characteristics (IVC). The finite R_0 is explained by QPS and shows an exponential dependence on $\sqrt{E_J/E_C}$ with a distinct change in the exponent at $R_0 = R_Q = h/4e^2$. When $R_0 > R_Q$, the IVC clearly shows a remnant of the Coulomb blockade, which evolves to a zero-current state with a sharp critical voltage as E_J is tuned to a smaller value. The zero-current state below the critical voltage is due to coherent QPSs and we show that these are enhanced when the central link is weaker than all other links. Above the critical voltage, a negative, differential resistance is observed, which nearly restores the zero-current state.

[4] Author to whom any correspondence should be addressed.

Contents

1. Introduction

An ideal superconductor has zero electrical resistance when it is cooled below a critical temperature T_C. However, a thin superconducting wire can exhibit non-zero resistance due to fluctuations of the superconducting order parameter which causes phase-slip events. The phase slip events can be thermally activated TAPS (thermally activated phase slips) [1, 2] or the result of quantum tunneling, QPS (quantum phase slip) [3–5]. In this paper we examine QPS in long Josephson junction chains where the phase-slip rate and the spatial location of phase slips along the chain are experimentally well controlled.

QPSs can be either incoherent or coherent. The former are dissipative, whereas the latter give rise to the Coulomb blockade of Cooper pair tunneling and Bloch oscillations in a Josephson junction [6], phenomena that are the electrodynamic dual to the dc and ac Josephson effects, respectively. Achieving this dual to the Josephson effect in a circuit which can support a dc electrical current is of fundamental interest for quantum metrology as it is predicted that Bloch oscillations could be synchronized to an external signal at frequency f, leading to a fundamental relation between electrical current and frequency, $I = 2ef$. Continuous systems that exhibit this dual state to superconductivity are thin films, where it has been called the 'superinsulator' state [7], and nanowires where there has been a long-standing interest in QPS and in the very existence of superconductivity in one dimension [3, 4, 8, 9]. Currently, there is a growing interest in realizing coherent QPS in nanowires as a possible dual element to the Josephson junction [10–12]. The Josephson junction series array is an artificial nanowire with great freedom of design. Here we demonstrate how this design freedom can be used to tune the rate of QPS uniformly along the array, as well as locally at one point in the middle of the array.

Series arrays have been previously studied as a model system for understanding QPSs and in particular their role in quantum phase transitions [13–15]. The series array can emulate an ideal superconducting nanowire when the array is long enough and uniform enough to hide its discrete nature, so that the probability per junction of QPS is relatively small and independent of position in the array. Classical simulations of phase slips in long arrays show that it is also necessary that the junction phase dynamics be overdamped in order for TAPS to occur uniformly along the array [16]. Underdamped dynamics results in persistent phase slips at random nucleation sites, as opposed to random TAPS occurring with equal probability along the array. QPSs have also been studied in short arrays [17–19] and here we extend these studies to longer arrays. We present measurements of dc electrical transport in long arrays where we are able to control the phase-slip rate uniformly along the array, and at one point in the middle of the array. We show that the zero-bias resistance R_0 is due to QPS. When phase slips are localized to a central weak link, the rest of the array essentially acts as tunable environment for the study of

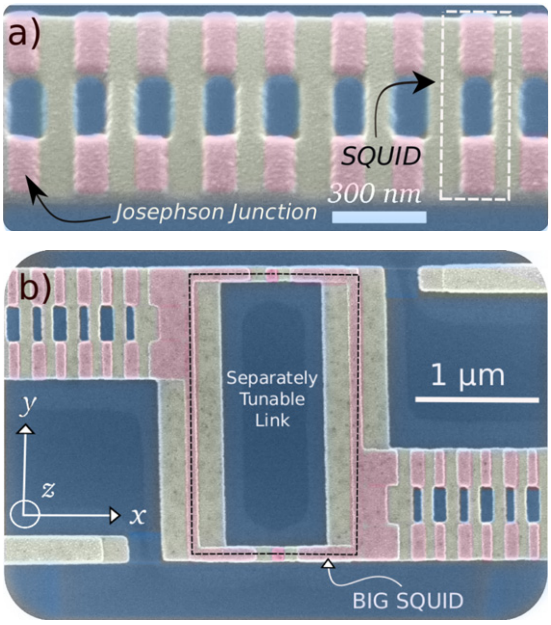

Figure 1. (a) Scanning electron microscope (SEM) image of a section of a uniform array when the beam is tilted ∼45° from normal incidence to the x–y plane of the sample. (b) SEM image with no tilt of the separately tunable link in the center of the chain. Compared the rest of the chain, the junctions of the big SQUID have lower I_{C0} due to the smaller junction size and I_C is tuned with a smaller period in magnetic field due to the larger loop size.

localized QPS. Localized QPSs in a circular array have recently been exploited in a promising new type of superconducting qubit [20–22].

When the junctions in the array are formed as dc superconducting quantum interference devices (SQUIDs), the rate of QPS can be tuned with an external magnetic field [17–19]. The SQUID chain is described as a series array along the x direction, where each junction is extended in the y direction and reformed into a loop with two parallel junctions (see figure 1). When an external magnetic field B_z is applied in the z direction, the effective Josephson coupling between the series SQUIDs is tuned with the magnetic flux threading each loop. The spatial dimensions transverse to the supercurrent flow are thus exploited to create a tunable one-dimensional system. However, this tunable coupling requires that the loop inductance is small enough, $L_{\rm loop}E_{\rm J0} \ll \left(\frac{\Phi_0}{2\pi}\right)^2$ such that the externally applied magnetic flux induces negligible circulating supercurrent in the loop, which is well satisfied in our chains.

When the Josephson coupling is tuned to zero, the chain is insulating and the important energy scale is the bare charging energy, which is fixed by the geometry of the islands in the chain. The electrostatic energy associated with one uncompensated charge sitting in the middle of a long chain will depend on the capacitance matrix of the chain which, for simplicity, is usually assumed to have a symmetric tridiagonal form, i.e. only nearest-neighbor capacitance C and capacitance to ground C_0 [23–25]. In this case the characteristic screening length of the field associated with this excess charge is $\Lambda = \sqrt{C/C_0}$, where $2C + C_0$ is the total capacitance of each island in the chain, and the energy required to put a quantum of charge in the middle of a neutral chain is $E_\Lambda = e^2/2\sqrt{CC_0}$.

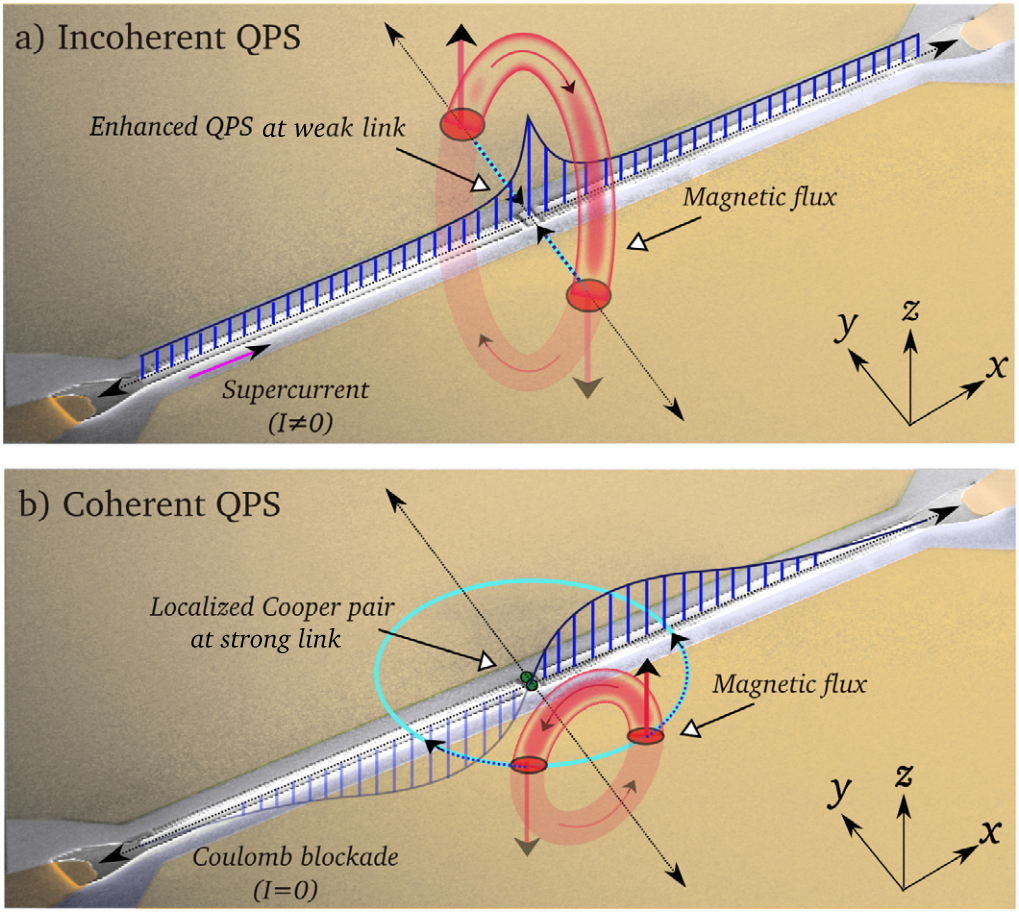

Figure 2. Artist's conception of incoherent (a) and coherent (b) QPS events. The QPS is associated with the tunneling of a magnetic flux quantum (red tubes) across the chain following the marked paths (green lines). The vertical blue bars represent the x component of the electric field (potential gradient) due to the time average of many QPSs. (a) Incoherent QPSs are enhanced at a weak link and in the presence of a finite supercurrent they give rise to dissipation in the chain. (b) Coherent QPSs describe a Coulomb blockade state where the current is zero. The potential gradient is due to an excess localized Cooper pair sitting at a strong link in the chain, where the effective island capacitance to ground is larger.

The superconducting state of the chain is characterized by a long-range order of the spatially distributed phase $\phi(x)$ of the complex order parameter. A supercurrent is associated with a finite phase gradient along the chain, $I_s = I_C \sin(a_0 \frac{d\phi}{dx})$, where a_0 is the distance between junctions in the chain. A phase slip is an event in which the phase at some point suddenly unwinds by 2π leading to a local change of the current and generation of a voltage pulse by the Josephson effects. We can also visualize a phase slip as a magnetic flux quantum crossing the chain, where the field associated with the flux, the direction of flux transport and the direction of supercurrent flow, are all orthogonal (see figure 2). When there is a finite supercurrent, an incoherent QPS is associated with dissipation of electromagnetic energy stored in the fields surrounding the chain and it can be visualized as the disappearance of a circulating tube

containing one quantum of magnetic flux (see figure 2(a)). In this process one flux quantum effectively crosses the chain, and the net effect of many random QPSs is a time-average potential gradient at the crossing point, or component of the electric field E_x, parallel to the supercurrent. This results in a Poynting vector with a component directed toward the chain.

Coherent QPSs are associated with a zero-current state with no dissipation, and they describe a Coulomb blockade below a finite critical voltage. If an excess Cooper pair sits at a strong link in the center of the chain, it will form an electrostatic potential $U(x)$ describing a Cooper pair charge soliton [17, 26, 27]. The electrostatic potential gradient, or x-component of the electric field $E_x = \frac{dU}{dx}$, is positive on one side of the charge, and negative on the other (see figure 2(b)). If the potential gradient is interpreted as flux motion crossing the chain, it corresponds to a vacuum fluctuation where a tube of circulating flux is created on one side of the chain, two opposing flux quanta traverse the chain on opposite sides of the charge, and are then annihilated. Thus a virtual flux quantum effectively circulates once around the charge (Aharonov–Casher effect [28, 29]) beginning and ending with a state of zero flux. The sign of the potential gradient and the direction of circulation in the flux tube depend on the sign of the uncompensated charge quantum (i.e. charge soliton or anti-soliton). Thus the QPSs avoid the central link if it is stronger than other links in the chain and the excess charge will find a lower energy at this point where there is an effectively larger island with larger capacitance to ground. Conversely, if the central link is weaker, coherent QPSs are enhanced and the charge avoids this point.

2. Experimental details

Long chains with as many as 4888 SQUIDS in series (9776 junctions—all working!) have been fabricated with electron beam lithography (EBL) by stitching several write fields together. A combination of automatic and manual techniques was used for write-field alignment with a laser interferometer stage (Raith 150 E-beam Lithography system), so that stitching errors did not affect the uniformity of junctions in the chain. The co-planar waveguide formed with these long chains (see figure 2) has a microwave impedance which is much higher than the leads terminating its ends and therefore the chain is well voltage biased at high frequencies relevant to phase dynamics. This impedance mismatch to the leads also means that internal junctions of the chain are rather immune to electromagnetic fluctuations in the leads. However, to provide more filtering and a better voltage bias, we fabricated a shunt capacitance to the ground planes (about 180 pF) on chip, close to each termination of the chain (120 μm distance, not seen in figure 2). The first layer of the shunt capacitors are Al rectangles defined by optical lithography on Si/SiO_2 substrate. An insulating oxide (Al_2O_3) was then formed by heavy plasma oxidation and a second layer of photolithography and Au deposition formed the ground planes on-chip leads.

The lift-off mask for the Josephson junction chain was made by EBL using a two-layer resist system with over-development of the bottom layer to obtain large undercut and rather long (≈ 1 μm) free-standing bridges. The junctions were then fabricated by two-angle Al evaporation with *in situ* oxidation to form overlapping Al islands with an Al_2O_3 tunnel barrier [30]. We have fabricated over 250 chains which showed some room temperature conductance. More than 40 with a wide variety of parameters have been measured in the cryostat. In this paper, we concentrate on describing measurements on five samples whose parameters are given in table 1. Samples 1–4 were uniform chains and details of the loop junctions can be seen in

Table 1. Parameters of the Josephson junction chains studied in this paper: N is the number of series links in the chain; A is the total area of two junctions in the loop which forms one link in the chain; $R_{\rm Tot}$ is the total normal state resistance of the chain; $R_{\rm N} = R_{\rm Tot}/N$ is the normal state resistance of each link in the chain, assuming a uniform chain; $E_{\rm J0}$ is the bare Josephson coupling energy of each link, determined from $R_{\rm N}$ and the superconducting energy gap Δ_0, $E_{\rm J0} = (R_{\rm Q}/R_{\rm N})(\Delta_0/2)$; $E_{\rm C}$ is the charging energy associated with the nearest-neighbor capacitance C, determined from the area A and the specific capacitance $c_{\rm S} = 45\,{\rm fF}\,\mu{\rm m}^{-2}$, $E_{\rm C} = e^2/(2c_{\rm S}A)$; $E_{\rm J0}/E_{\rm C}$ is the ratio between two characteristic energies at zero external magnetic field. The island stray capacitance is estimated to be $C_0 \approx 15\,{\rm aF}$.

Parameters	N	A	$R_{\rm Tot}$	$R_{\rm N}$	$E_{\rm J0}$	$E_{\rm C}$	$E_{\rm J0}/E_{\rm C}$
Units	#	$\mu{\rm m}^2$	MΩ	kΩ	μeV	μeV	#
Sample 1	2888	0.05	1.88	0.65	990	35.6	27.8
Sample 2	384	0.06	0.28	0.72	890	29.6	30
Sample 3	2888	0.05	1.43	0.5	1302	35.6	36.6
Sample 4	2888	0.02	0.2	0.0817	7898	88.8	88.7
Sample 5 (chain)	384	0.06	0.86	2.24	288	29.6	9.7
Sample 5 (tunable-link)	1	0.02	0.00672	6.72	96	88.8	1.08

figure 1(a). The co-planar wave guide has capacitance per unit length $75\,{\rm aF}\,\mu{\rm m}^{-1}$ (center strip width $1\,\mu$m, gap $5\,\mu$m, effective dielectric of the SiO_2/Si substrate $\epsilon = 9.25$). Multiplying this by the separation between islands, $0.2\,\mu$m, we approximate $C_0 \simeq 15\,{\rm aF}$. The two parallel junctions in each SQUID were rather large ($300 \times 100\,{\rm nm}$) giving $C \simeq 2.7\,{\rm fF}$, or $\sqrt{C/C_0} \cong 13$.

Sample 5 had a separately tunable link fabricated at the center of the chain, which was realized by a loop with smaller junctions and larger loop area (figure 1(b)). The larger loop area allows for the coupling energy of the center link to be tuned with a period in magnetic field that is different from the links in the chain. The modulation of transport is periodic in the externally applied magnetic field B_z, having a period of one flux quantum $\Phi_0 = \frac{h}{2e}$ for each loop area A in the chain. The effective Josephson coupling is given by $E_{\rm J} = E_{\rm J0}|\cos(\pi B_z A/\Phi_0)|$. Here $E_{\rm J0} = \frac{R_{\rm Q}}{R_{\rm N}}\frac{\Delta_0}{2}$ is the zero-magnetic-field value of the Josephson coupling, $R_{\rm N}$ is the normal state resistance of each link in the chain, $\Delta_0 = 200\,\mu$eV is the $T = 0$ superconducting energy gap and $R_{\rm Q} = \frac{\Phi_0}{2e} = 6.45\,{\rm k}\Omega$ the quantum impedance. Measuring this periodicity directly as a function of the current in our magnet allows us to accurately determine $E_{\rm J}(B_z)$ from a calculated value of $E_{\rm J0}$.

After lift-off and initial testing the sample chip is wire bonded to a printed circuit board with microwave connectors and mounted in an RF tight copper can. Measurements were made in a dilution refrigerator with a base temperature of $\approx 15\,{\rm mK}$. Figure 3 shows a schematic diagram of the measurement circuit. The measurement leads from room temperature to the RF connectors on the copper can were about 2.5 m of continuous (no connectors) lossy micro coax cables with $50\,\Omega$ impedance. These cables have poor thermal conductance (CuNi, 0.4 mm outer diameter) and large microwave attenuation ($61\,{\rm dB\,m}^{-1}$ @ $10\,{\rm GHz}$) and thereby provide some thermalization of the microwave field fluctuations toward the base temperature of the cryostat.

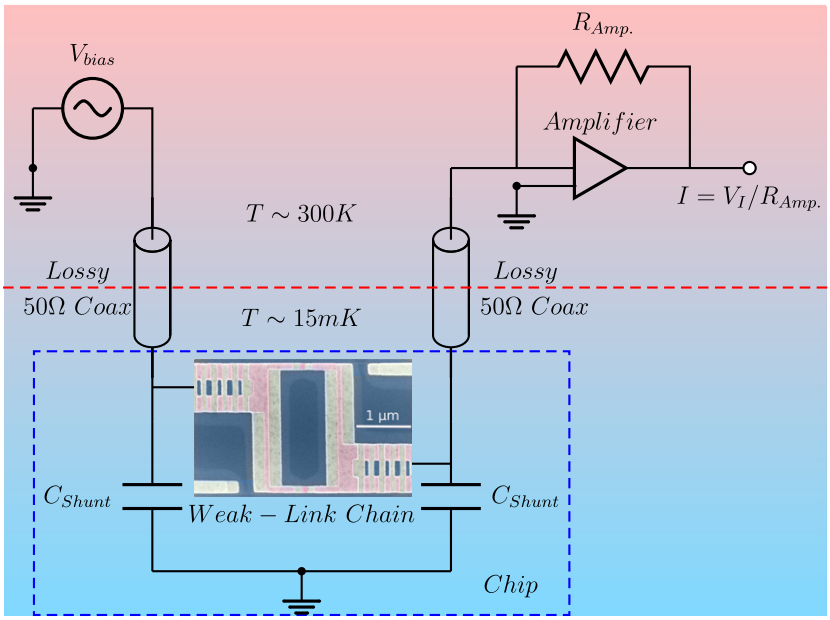

Figure 3. Schematic diagram of the measurement circuit.

3. Results and analysis

The current–voltage characteristics (IVC) of sample 4 at zero magnetic field and various temperatures are shown in figure 4(a). The IVCs consist of a supercurrent-like branch with a finite slope R_0 at low-bias voltages, followed by a peak and a constant current branch at high-bias voltages. The peak and constant current branch are reproduced by simulation of TAPS, where the constant current branch is due to a continuous and random slipping and sticking of the phase, occurring uniformly along the chain [16]. However, simulations show that the resistance of the supercurrent-like branch, or R_0 due to TAPS, is much smaller than that measured in experiment. The measured temperature dependence of R_0 plotted in figure 4(b) shows a nearly temperature-independent 'flat tail' below the superconducting transition temperature of Al, with a slight *increase* in R_0 as temperature is decreased (figure 4(b) inset). Resistance due to TAPS would have the opposite behavior of increasing R_0 with increasing temperature. The increase of R_0 at low temperatures in the chains can be qualitatively explained as being due to QPS within the context of a model for quantum phase transitions [31], and a similar superconducting–insulating transition is also observed for thin superconducting wires [32].

The large value of R_0 and its weak temperature dependence tell us that the majority of the phase slips are QPSs[5]. The tunneling amplitude Γ of QPS depends on the ratio of the Josephson coupling energy to the charging energy, E_J/E_C [5, 33]. In the case of a Josephson junction chain in the limit where $E_J \gg E_C$, $C \gg C_0$, and no random offset charges, one may estimate Γ as [33]

$$\Gamma = \sqrt{\frac{2}{\pi}} N\hbar\Omega\sqrt{S}\,\mathrm{e}^{-S}, \tag{1}$$

$$S = \sqrt{8E_J/E_C}, \tag{2}$$

[5] In the case of TAPS we would have expected to see a different kind of exponential dependence, $R_0 \propto \exp(-2E_J/(k_B T))$. By fitting the R_0 versus E_J data of sample 2 we obtain $T \approx 6.7\,\mathrm{K} \gg T_C$.

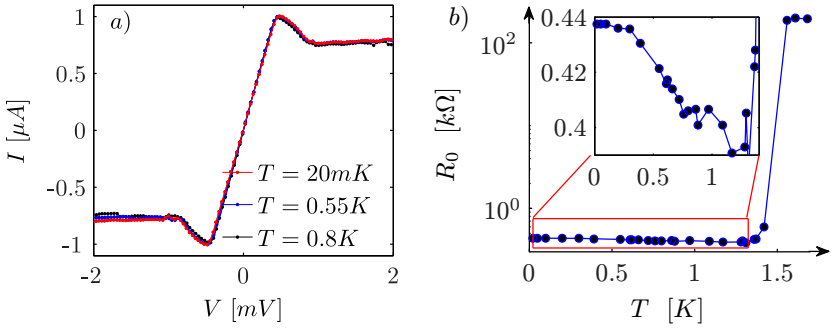

Figure 4. (a) Various dc IV curves of sample 4 between the $T = 20$ mK and 0.8 K at zero magnetic field. (b) Zero-bias resistance as a function of temperature and the inset shows the zoom to the *flat-tail*.

where S is the action for an instanton connecting two neighboring minima and $\Omega = \sqrt{8E_J E_C}/\hbar$ is the plasma frequency of the Josephson junction. Interestingly, the same expression for Γ holds for a single junction if one omits the N in the prefactor. For finite C_0, and long chains with $N \gg \Lambda$, one expects an additional contribution $\sim\pi\sqrt{E_J/8E_C\Lambda^2}\ln(N/\pi\Lambda)$ to S, which, however, becomes negligible when $E_J \gg E_{C0} = E_C\Lambda^2$ [19]. If random offset charges are present, as they may well be in our experiments, the linear scaling with N is predicted to cross over to a $\sqrt{N}$ dependence for large N [33].

A reasonable assumption is that the zero-bias resistance $R_0 \sim$ the number of phase slip events per time, i.e. the *rate* of QPSs. This in turn is proportional to the absolute square of the tunneling amplitude $|\Gamma|^2$, multiplied by the density of states of the environment. In effect we then get, in the limit $E_J \gg E_C$, a resistance $R_0 \sim \exp(-2S)$, neglecting prefactors. In practice, there is also some uncertainty in our estimates of E_J and E_C, and we therefore model our experiments using

$$R_0 \propto e^{-\alpha\sqrt{E_J/E_C}}, \tag{3}$$

where α is treated as a fitting parameter. Figure 5 displays $\log R_0$ versus $\sqrt{E_J/E_C}$ for samples 1–3 which are uniform chains, and for sample 5 which contains the separately tunable link in the middle of the chain. The uniform chains do indeed follow the exponential dependence of equation (3) in the large E_J limit. Surprisingly, the same exponential relation holds in the lower E_J limit, but with a different α value. We observe a clear transition between different exponential factors $\alpha_{low} = 1.16$ and $\alpha_{high} = 4.75$, when the zero-bias resistance approximately equals the resistance quantum ($R_0 \approx R_Q$). This happens around $\sqrt{E_J/E_C} \approx 4$. Note also that although these uniform chains have very different numbers of junctions N, they have essentially identical dependence of R_0 on $\sqrt{E_J/E_C}$. Apparently, these long chains are not influenced by the chain length, which is contrary to earlier R_0 measurements on shorter chains [31]. This independence of chain length might indicate that the scaling is influenced by proximity of the superconductor–insulator transition, where the additional logarithmic N dependence of S (see the discussion below equation (2)), becomes important and, in principle, could compensate the scaling of the prefactor for a range of E_J/E_C [19].

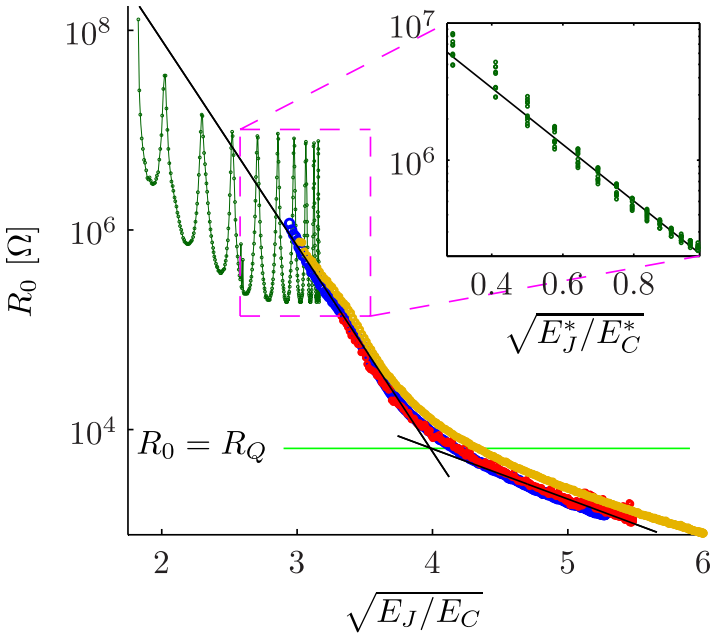

Figure 5. Zero-bias resistance plotted as a function of $\sqrt{E_J/E_C}$ for samples 1, 2, 3 and 5 (blue, red, orange and dark green points, respectively). The black solid lines have slopes $\alpha_{low} = 1.16$ for $\sqrt{E_J/E_C} > 4$ and $\alpha_{high} = 4.75$ for $\sqrt{E_J/E_C} < 4$. Inset shows the R_0 modulation of the sample 5 as a function of $\sqrt{E_J^*/E_C^*}$ of the separately tunable link. The slope of the black line in the inset is also $\alpha_{high} = 4.75$.

Also shown in figure 5 is sample 5 with the separately tunable link. The rapid modulation of R_0 seen in this sample is due to modulation of E_J^* of the central link, whereas the change in the average R_0 is due to modulation of E_J of the chain. Since the modulation is much faster for the central link than for the chain junctions, the rapid oscillations of R_0 become quasi-periodic when plotted against $\sqrt{E_J/E_C}$ of the chain. In the region where the chain $\sqrt{E_J/E_C} < 2.5$ the effect of the modulation of the chain junctions becomes visible. At the maximum points in this region, where the central link E_J^* is at a minimum, R_0 fall close to the line with the same value of $\alpha_{high} = 4.75$ found for the uniform chains. At these maxima QPSs appear to be as for a uniform chain. Conversely, at the minima of R_0 in this region, where E_J^* of the central link is maximum, we see how a strong link in the center of the chain can cause a significant drop in the R_0 of the chain. In the region $2.5 < \sqrt{E_J/E_C} < 3.2$ the chain junctions have essentially constant $\sqrt{E_J/E_C}$ and R_0 is mostly influenced by the modulation of the central link. We plot log R_0 versus $\sqrt{E_J^*/E_C^*}$ of the central link in the inset of figure 5, where we see an exponential behavior according to equation (3) with the same slope $\alpha_{high} = 4.75$.

The transition at $R_0 \simeq R_Q$ with its associated change in the exponent α is also accompanied by a qualitative change in the nonlinear character of the IVC. Figure 6 shows the IVC and the differential conductance of sample 2 measured at either side of the transition. When $R_0 < R_Q$, the differential conductance displays a single peak at zero bias (figure 6(b)). However, when $\sqrt{E_J/E_C}$ is tuned so that $R_0 > R_Q$, we see a dip in the differential conductance at zero bias (figure 6(d)). This dip is a remnant of the Coulomb blockade which is heavily smeared by quantum fluctuations of the quasicharge (incoherent Cooper pair tunneling) [34]. As the

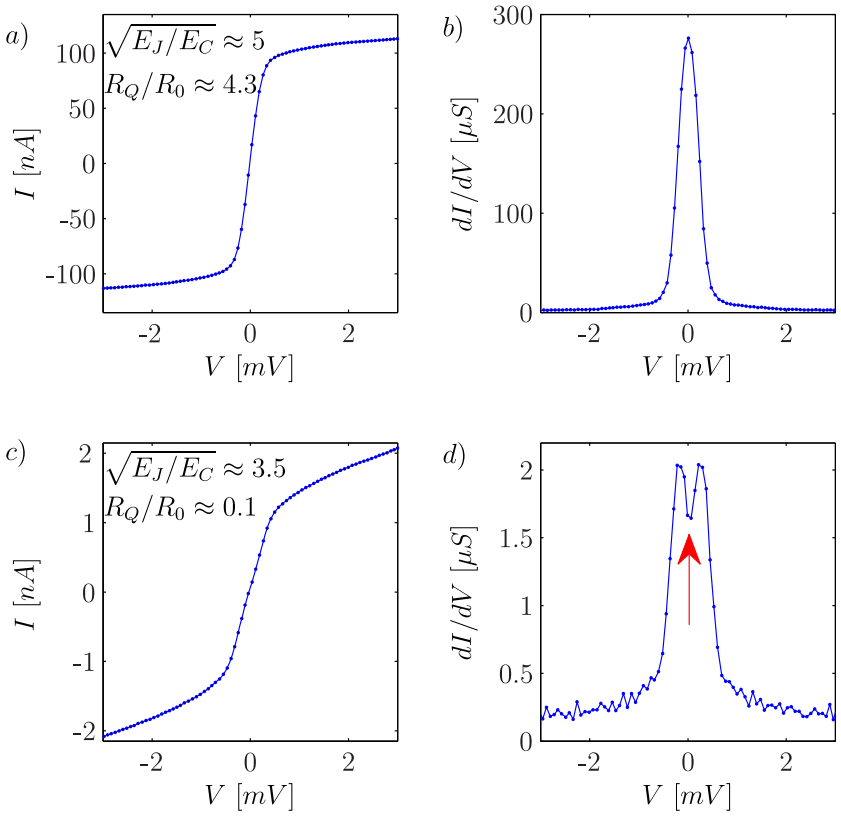

Figure 6. Dc *IV* curve (a) and differential conductance (b) of sample 2 as a function of bias voltage at $\sqrt{E_J/E_C} \approx 5$ and $R_Q/R_0 \approx 4.3$. Dc *IV* curve (c) and differential conductance (d) of the same sample at $\sqrt{E_J/E_C} \approx 3.5$ and $R_Q/R_0 \approx 0.1$. The differential conductance curve shows the suppression of the zero-bias conductance and the remnant of the Coulomb blockade state (red arrow).

magnetic field is increased and E_J is suppressed further, this dip develops into a true zero current state with an E_J dependent critical voltage.

Samples 1–3 showed this transition in the IVC as the zero-bias resistance crossed R_Q. Sample 5 with the separately tunable link showed a zero-bias dip in the differential conductance at *all* magnetic fields due to the small $\sqrt{E_{J0}^*/E_C^*}$ of the separately tunable junction. Sample 5 has two different loop sizes and its differential conductance therefore shows a rich dependence on magnetic field and bias voltage, shown as a color map in figure 7(a). The pattern with period 7.5 G corresponds to one flux quantum in the larger loop of the central link. Below 50 G, the zero-bias dip in differential conductance is clearly visible as a small white diamond feature around $V = 0$ at magnetic fields where the coupling in the central junction E_J^* is suppressed to a minimum. At magnetic fields above 50 G, E_J of the chain junctions begins to be suppressed, causing the impedance of the chain to increase and the small diamond feature to grow in size as the Coulomb blockade in the central junction is enhanced. Above 70 G the Coulomb blockade in the chain starts to take over with a rapidly increasing critical voltage which reaches a maximum at 90 G, where E_J of the chain junctions is at a minimum.

A very interesting feature occurs at 76.8 G, where the central link coupling E_J^* is at a minimum and the chain has a well-developed Coulomb blockade (see figure 7(b)). The IVC is

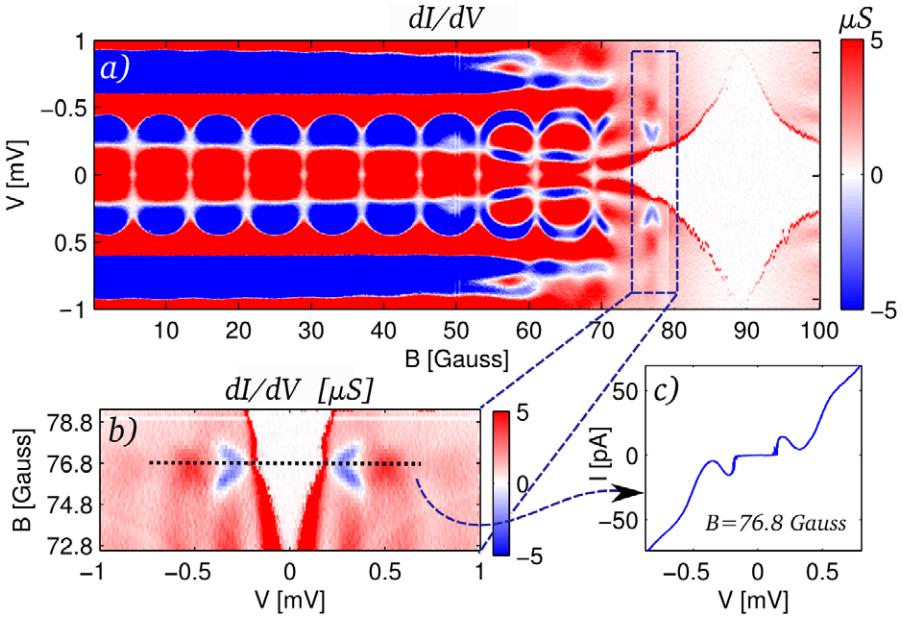

Figure 7. (a) Color map of the differential conductance of sample 5 as a function of magnetic field and bias voltage. The periodic pattern with period 7.5 G corresponds to one flux quantum in the large loop of the centre-link junction. (b) Zoom to the region where the chain impedance increases such that the IVC is determined by both the chain and the centre link. It is also possible to see the enhancement of the Coulomb gap due to the centre link at $B \approx 76.8$ G. (c) Dc IV curve of the sample at $B = 76.8$ G.

shown in figure 7(c) and it displays the classic signs of coherent QPS: a well-developed zero-current state and distinct critical voltage that varies with E_J. The critical voltage shows a small increase at this magnetic field, signaling that coherent QPSs are more frequent at the central link as they contribute by a noticeable amount to the total critical voltage. When the chain is biased above the critical voltage, there is a sharp onset of Cooper pair tunneling, followed by a region with negative differential resistance (NDR) reaching a nearly zero-current state. Noteworthy is the region with NDR as it tells us that coherent QPSs are happening in the presence of a low-dissipation environment. Indeed, we have seen in simulations of classical phase slips in chains with a central weak link that this NDR occurs when the phase slip rate at the central link exceeds the plasma frequency of the chain junctions, where a gap is predicted in the electromagnetic mode spectrum of the chain [35, 36]. This gap prevents the excitation of the chain modes and coherent QPSs can occur above the threshold voltage, where a dc current can flow. This interpretation means that the current in this region of NDR is characterized by underdamped Bloch oscillations.

4. Conclusion

We demonstrated the spatial and temporal control of incoherent and coherent QPSs in long, tunable Josephson junction SQUID chains. Incoherent QPSs give a zero-bias resistance which is well described by simple exponential behavior, $R_0 \propto \exp(-\alpha\sqrt{E_J/E_C})$. This dependence is consistent with theoretical estimates based on QPS in the limit of large E_J/E_C and vanishing

ground capacitors. Interestingly, a crossover to another regime ($E_J \lesssim 16E_C$) with the same type of exponential behavior, but a higher value of α, occurs around the resistance quantum $R_Q = h/4e^2$. In the IVC, the crossover is accompanied by the appearance of a zero-bias anomaly which is a remnant of the Coulomb blockade of Cooper pair tunneling. This qualitative change at $R_0 = R_Q$ represents a crossover to a regime $R_0 > R_Q$ where QPSs are strongly interacting and start to develop coherence. A theory for this regime is currently lacking. Although the chains are very uniform and QPS could happen anywhere, we observe no strong length dependence of either the exponent α or the prefactor of the exponential. Previous measurements on shorter chains showed very clear finite-size effects [31].

Coherent QPSs are realized when E_J is further suppressed and the zero-bias anomaly in the IVC develops into a zero-current state with a critical voltage that depends on E_J. We find that when this critical voltage is enhanced by an increased rate of coherent QPS at a weak link in the center of the chain, there appears a very interesting NDR in the IVC above the critical voltage. We speculate that this NDR is due to underdamped Bloch oscillations in the chain. Understanding the nature of this state of the chain dynamics could provide an insight into how one might structure coherent QPS along a chain, and provide a clue as to how to design a chain where Bloch oscillations can be synchronized to an external electromagnetic signal.

Acknowledgments

We gratefully acknowledge financial support from the EU project SCOPE and the Swedish Research Council VR.

References

[1] McCumber D E and Halperin B I 1970 Time scale of intrinsic resistive fluctuations in thin superconducting wires *Phys. Rev.* B **1** 1054–70
[2] Langer J S and Ambegaokar V 1967 Intrinsic resistive transition in narrow superconducting channels *Phys. Rev.* **164** 498–510
[3] Giordano N 1988 Evidence for macroscopic quantum tunneling in one-dimensional superconductors *Phys. Rev. Lett.* **61** 2137–40
[4] Bezryadin A, Lau C N and Tinkham M 2000 Quantum suppression of superconductivity in ultrathin nanowires *Nature* **404** 971–4
[5] Arutyunov K Yu, Golubev D S and Zaikin A D 2008 Superconductivity in one dimension *Phys. Rep.* **464** 1–70
[6] Averin D V, Zorin A B and Likharev K K 1984 Bloch oscillations in small Josephson junction *Zh. Eksp. Teor. Fiz.* **88** 407–12
[7] Vinokur V M, Baturina T I, Fistul M V, Mironov A Yu, Baklanov M R and Strunk C 2008 Superinsulator and quantum synchronization *Nature* **452** 613–5
[8] Lau C N, Markovic N, Bockrath M, Bezryadin A and Tinkham M 2001 Quantum phase slips in superconducting nanowires *Phys. Rev. Lett.* **87** 217003
[9] Golubev D S and Zaikin A D 2001 Quantum tunneling of the order parameter in superconducting nanowires *Phys. Rev.* B **64** 014504
[10] Mooij J E and Nazarov Yu V 2006 Superconducting nanowires as quantum phase-slip junctions *Nature Phys.* **2** 169–72
[11] Astafiev O V, Ioffe L B, Kafanov S, Pashkin Yu A, Arutyunov K Yu, Shahar D, Cohen O and Tsai J S 2012 Coherent quantum phase slip *Nature* **484** 355
[12] Lehtinen J S, Zakharov K and Arutyunov K Yu 2012 Coulomb blockade and Bloch oscillations in superconducting Ti nanowires *Phys. Rev. Lett.* **109** 187001

[13] Bradley R M and Doniach S 1984 Quantum fluctuations in chains of Josephson junctions *Phys. Rev.* B **30** 1138–47
[14] Sondhi S L, Girvin S M, Carini J P and Shahar D 1997 Continuous quantum phase transitions *Rev. Mod. Phys.* **69** 315–33
[15] Rosario F and van der Zant H S J 2001 Quantum phase transitions and vortex dynamics in superconducting networks *Phys. Rep.* **355** 235–334
[16] Ergül A, Lidmar J, Johansson J, Schaeffer D, Lindblom M and Haviland D B 2013 Phase-sticking in one-dimensional Josephson junction chains arXiv:1304.4046 [cond-mat.mes-hall] at press
[17] Haviland D B, Andersson K and Ågren P 2000 Superconducting and insulating behavior in one-dimensional Josephson junction arrays *J. Low Temp. Phys.* **118** 733–49
[18] Pop I M, Protopopov I, Lecocq F, Peng Z, Pannetier B, Buisson O and Guichard W 2010 Measurement of the effect of quantum phase slips in a Josephson junction chain *Nature Phys.* **6** 589–92
[19] Rastelli G, Pop I M and Hekking F W J 2013 Quantum phase slips in Josephson junction rings *Phys. Rev.* B **87** 174513
[20] Manucharyan V E, Koch J, Glazman L I and Devoret M H 2009 Fluxonium: single Cooper-pair circuit free of charge offsets *Science* **326** 113–6
[21] Manucharyan V E, Masluk N A, Kamal A, Koch J, Glazman L I and Devoret M H 2012 Evidence for coherent quantum phase slips across a Josephson junction array *Phys. Rev.* B **85** 024521
[22] Ferguson D G, Houck A A and Koch J 2013 Symmetries and collective excitations in large superconducting circuits *Phys. Rev.* X **3** 011003
[23] Bakhvalov N S, Kazacha G S, Likharev K K and Serdyukova S I 1989 Single-electron solitons in one-dimensional tunnel structures *Sov. Phys.—JETP* **68** 581–7
[24] Korotkov A N, Averin D V and Likharev K K 1994 Combined bloch/set oscillations in 1D arrays of small tunnel junctions *Physica* B **194–196** 1333–4
[25] Hu G Y and O'Connell R F 1994 Exact solution for the charge soliton in a one-dimensional array of small tunnel junctions *Phys. Rev.* B **49** 16773–6
[26] Hermon Z, Ben-Jacob E and Schön G 1996 Charge solitons in one-dimensional arrays of serially coupled Josephson junctions *Phys. Rev.* B **54** 1234–45
[27] Haviland D B and Delsing P 1996 Cooper-pair charge solitons: the electrodynamics of localized charge in a superconductor *Phys. Rev.* B **54** R6857–60
[28] Elion W J, Wachters J J, Sohn L L and Mooij J E 1993 Observation of the Aharonov–Casher effect for vortices in Josephson-junction arrays *Phys. Rev. Lett.* **71** 2311–4
[29] Grosfeld E and Stern A 2011 Observing Majorana bound states of Josephson vortices in topological superconductors *Proc. Natl Acad. Sci. USA* **108** 11810–4
[30] Dolan G J 1977 Offset masks for lift-off photoprocessing *Appl. Phys. Lett.* **31** 337–9
[31] Haviland D B, Andersson K, Ågren P, Johansson J, Schöllmann V and Watanabe M 2001 Quantum phase transition in one-dimensional Josephson junction arrays *Physica* C **352** 55–60
[32] Bezryadin A 2008 Quantum suppression of superconductivity in nanowires *J. Phys.: Condens. Matter* **20** 043202
[33] Matveev K A, Larkin A I and Glazman L I 2002 Persistent current in superconducting nanorings *Phys. Rev. Lett.* **89** 096802
[34] Ingold G L and Nazarov Y V 1992 Charge tunneling rates in ultrasmall junctions *Single Charge Tunneling* (*NATO ASI Series B, 21* vol 294) ed H Grabert and M H Devoret (New York: Plenum) pp 21–107 (also available at arXiv:cond-mat/0508728v1)
[35] Hutter C, Tholén E A, Stannigel K, Lidmar J and Haviland D B 2011 Josephson junction transmission lines as tunable artificial crystals *Phys. Rev.* B **83** 014511
[36] Masluk N A, Pop I M, Kamal A, Minev Z K and Devoret M H 2012 Microwave characterization of Josephson junction arrays: implementing a low loss superinductance *Phys. Rev. Lett.* **109** 137002